Published in final edited form as:

Cancer Res. 2015 June 15; 75(12): 2501–2509. doi:10.1158/0008-5472.CAN-14-3361.

Breast Cancer Detection by B7-H3 Targeted Ultrasound Molecular Imaging

Sunitha V. Bachawal[1], **Kristin C. Jensen**[2], **Katheryne E. Wilson**[1], **Lu Tian**[3], **Amelie M. Lutz**[1], and **Jürgen K. Willmann**[1]

[1]Department of Radiology, Molecular Imaging Program at Stanford, Stanford University School of Medicine, Stanford, California, USA

[2]Departments of Pathology, Stanford University, Stanford, California, USA and Veterans Affairs Palo Alto Health Care System

[3]Department of Health, Research & Policy, Stanford University, Stanford, California, USA

Abstract

Ultrasound complements mammography as an imaging modality for breast cancer detection, especially in patients with dense breast tissue, but its utility is limited by low diagnostic accuracy. One emerging molecular tool to address this limitation involves contrast-enhanced ultrasound using microbubbles targeted to molecular signatures on tumor neovasculature. In this study, we illustrate how tumor vascular expression of B7-H3 (CD276), a member of the B7 family of ligands for T cell co-regulatory receptors, can be incorporated into an ultrasound method that can distinguish normal, benign, precursor and malignant breast pathologies for diagnostic purposes. Through an immunohistochemical analysis of 248 human breast specimens, we found that vascular expression of B7-H3 was selectively and significantly higher in breast cancer tissues. B7-H3 immunostaining on blood vessels distinguished benign/precursors from malignant lesions with high diagnostic accuracy in human specimens. In a transgenic mouse model of cancer, the B7-H3-targeted ultrasound imaging signal was increased significantly in breast cancer tissues and highly correlated with ex vivo expression levels of B7-H3 on quantitative immunofluorescence. Our findings offer a preclinical proof of concept for the use of B7-H3-targeted ultrasound molecular imaging as a tool to improve the diagnostic accuracy of breast cancer detection in patients.

Corresponding Author: Jürgen K. Willmann, M.D., Department of Radiology, Molecular Imaging Program at Stanford, School of Medicine, Stanford University, 300 Pasteur Drive, Room H1307, Stanford, CA 94305-5621, P: 650-723-5424; Fax: 650-723-1909, willmann@stanford.edu.

Conflicts of Interest: None

Authors' Contributions:

Conception and design: Jürgen K. Willmann, MD; Sunitha V. Bachawal, PhD

Development of methodology: Jürgen K. Willmann, MD; Sunitha V. Bachawal, PhD

Acquisition of data: Sunitha V. Bachawal, PhD, Kristin Jensen, MD, Katheryne E Wilson, Amelie M. Lutz, MD; Jürgen K. Willmann, MD

Analysis and interpretation of data: Sunitha V. Bachawal, PhD; Kristin Jensen, MD, Amelie M. Lutz, MD; Lu Tian, PhD; Jürgen K. Willmann, MD

Writing, review and/or revision of the manuscript: All authors

Study supervision: Jürgen K. Willmann, MD

Keywords

CD276; B7-H3; Targeted ultrasound imaging; breast cancer; microbubbles

INTRODUCTION

Breast cancer is the second leading cause of cancer-related deaths in women in the United States, with an estimated 232,670 new diagnoses and 40,000 deaths from this cancer in 2014 (1). If detected early, survival of women with breast cancer can be substantially increased compared to detection at later stages. The 5-year survival rate in patients diagnosed with stage I and II disease is 100% and 98.5% compared to 84.6% and 25.0, respectively, when detected at stage III and IV disease (1). Next to breast self-exam and clinical breast exam, the American Cancer Society recommends mammography as a screening exam in women age 40 and older (2). For high risk women, mammography is recommended at age 30 years (2).

However, presence of dense or heterogeneously dense breast tissue, which is particularly prevalent in younger patients (3), may decrease diagnostic accuracy of mammography in detecting breast cancer, with sensitivities ranging between 30% and 55% (4–6). Adding ultrasound to screening mammography is currently being explored as a complementary screening approach for earlier breast cancer detection in women with dense breast tissue (7). Several studies have addressed the value of adding breast ultrasound imaging to screening mammography and demonstrated an increase in cancer detection rates ranging from 0.3 to 7.7 cancers per 1000 women screened (6–11). Berg *et al*., showed that breast cancer was diagnosed on ultrasound alone in 12 of 40 patients (30%) (11). However, the diagnostic accuracy of current ultrasound screening techniques in breast cancer detection is low with a positive predictive value (PPV) as low as 8.6% (11) or even lower 5.6% in another study (12), resulting in a large number of unnecessary callbacks and biopsies. In addition, the sensitivity of ultrasound performed alone in detecting invasive breast cancer was only 50% (11) and 27% in another prospective multimodality screening study (13). Therefore, further improvement of the diagnostic accuracy of ultrasound imaging is critically needed for women enrolled in breast cancer screening.

Molecularly-targeted contrast enhanced ultrasound imaging is an emerging imaging strategy with large potential for improving diagnostic accuracy of conventional ultrasound imaging in earlier cancer detection (14–16). Ultrasound contrast agents are gas filled echogenic microbubbles that can be further modified by adding binding ligands to the microbubble shell, which makes them firmly attach to molecular markers (17, 18). Since microbubbles are several micrometers in size they remain exclusively within the vascular compartment (18). This property of a purely intravascular contrast agent makes them particularly well suited for visualizing molecular markers expressed on the tumor neovasculature in various cancers, including breast cancer (16, 19). To achieve both high sensitivity and specificity in detecting breast cancer with ultrasound, it is of paramount importance to identify molecular markers as potential molecular imaging targets that are differentially expressed on the neovasculature of cancer compared to normal tissue, benign and precursor breast lesions.

Extensive research is under way aimed at identifying such cancer-specific vascular markers using various discovery techniques for both imaging and therapeutic purposes (20). Using a serial analysis of gene expression (SAGE) technique on isolated vascular endothelial cells, the transmembrane protein B7-H3, also known as CD276, was discovered as a novel tumor neovasculature associated marker differentially expressed in murine and human colon, breast, and lung cancer xenografts grown in mice (21). Recently, the B7-H3 protein was shown to be expressed in human breast cancer tissues (22). However, it is not known whether B7-H3 is differentially expressed on the neovasculature of breast cancer compared to benign, or precursor breast pathologies and normal breast tissue, which would make B7-H3 an attractive novel molecular imaging target for breast cancer detection using ultrasound.

The purpose of our study was twofold (Figure. 1): First, to evaluate B7-H3 expression on the tumor neovasculature of breast cancer versus normal tissue, benign and precursor breast lesions in a large scale human immunohistochemical analysis study and, second, to assess feasibility of ultrasound molecular imaging using new B7-H3-targeted contrast microbubbles for breast cancer detection in a genetically engineered mouse model.

MATERIALS AND METHODS

Figure. 1 summarizes the overall study design.

Collection of Human Breast Tissues

Human breast tissue samples were obtained retrospectively and were selected under an HIPAA compliant, IRB approved protocol to represent a range of normal tissue, benign and precursor lesions and cancer tissues. A total of 248 samples were obtained, including 101 breast cancer samples, 100 benign or precursor pathologies, and 47 normal breast tissues (Table 1). 209 samples were processed into a breast tissue microarray (TMA) using standardized protocols (23). In brief, tissue microarray cases were constructed from patient resection (surgical) tissues after characterization by a dedicated breast pathologist. Lesional areas were circled and 0.6-mm blocks were cored out from formalin-fixed paraffin-embedded tissue blocks by using a Beecher Tissue Microarrayer (Sun Prairie, WI), and then slotted in a regular grid pattern into a blank recipient paraffin wax block. Thirty-nine whole tissue samples of breast cancer were obtained from diagnostic large core needle biopsies. In these 39 whole tissue cancer samples, benign tissues adjacent to breast cancer were used as intra-individual benign control tissues.

Immunohistochemical Staining and Analysis of B7-H3 Expression in Human Breast Tissue Samples

Immunohistochemistry was performed on standard serial 5 μm sections of paraffin-embedded breast tissues using the Leica Bond Max automated platform (Leica Microsysytems Inc., IL). This platform was used in conjunction with a heat induced epitope retrieval program using an epitope retrieval solution (2, ER2; Leica Microsysytems Inc., IL) at pH 9.0. Antibodies to both human CD31 (clone JC70A at a 1:150 dilution; Dako, CA; to confirm presence on tumor vessels) and to human B7-H3 (AF1027, at 1:200 dilution; R&D systems, MN) were used on the same automated platform. Slides were imaged using a

digital slide scanner (Nanozoomer; Hamamatsu, SJ, CA). All immunohistochemically stained sections were analyzed by a dedicated breast pathologist. B7-H3 expression on tumor associated vascular endothelial cells was analyzed using adjacent CD31 stained slices for anatomical guidance to determine presence of tumor vessels. Immunostaining of vessels was scored using a 4-point grading scale: 0 = no staining; 1 = weak; 2 = moderate; and 3 = strong vessel staining. Vessel staining was further analyzed for percentage positive vessels using a 5-point grading scale: 0 = no positive staining vessels; 1 = 1–10%; 2 = 10–33%; 3 = 33–66%; and 4 = 66–100% of positive staining vessels. The results obtained by these two scores were then multiplied together yielding a single value as described (24). In addition, microvessel density (MVD) was calculated on all sections using standard techniques (25).

Cell Culture Experiments

Wild type MS1 ($MS1_{wt}$; American Type Culture Collection ATCC, Manassas, VA) vascular endothelial cells were transfected with B7-H3 expression vector using lipofectamine 2000 (Invitrogen, USA) to generate stable MS1 clones ($MS1_{B7\text{-}H3}$) and were maintained in culture under sterile conditions in a 5% CO_2-humidified atmosphere at 37°C in Dulbecco's Modified Eagle's Medium and supplemented with 10% fetal bovine serum and 100 U/mL penicillin and 100 μg/mL streptomycin. Cells were harvested by using trypsinization at 70%–80% confluence. Routine morphological analysis under microscope and growth curve analysis were performed to ensure consistent growth properties and authentication according to the ATCC cell line verification test recommendations. The expression of B7-H3 in transfected cells was tested by immunofluorescence imaging with anti-B7-H3 antibody.

Preparation of Targeted and Control Microbubbles

Commercially available streptavidin-coated microbubbles (VisualSonics, Toronto, Canada) were used to generate B7-H3-targeted microbubbles ($MB_{B7\text{-}H3}$) and control microbubbles ($MB_{Control}$). For further details please refer to Supplementary Methods

Flow Chamber Experiments

Binding specificity of $MB_{B7\text{-}H3}$ to the target B7-H3 was first assessed in cell culture experiments under flow shear stress conditions simulating flow in blood capillaries by using a flow chamber experimental set-up. Detailed description of experimental protocol is provided under Supplementary Methods.

Transgenic Mouse Model

All procedures involving the use of laboratory animals were approved by the Institutional Administrative Panel on Laboratory Animal Care. The well-established transgenic mouse model of breast cancer (FVB/N-Tg(MMTV-PyMT)634Mul) was used for all imaging experiments (16, 26). Breast tissue from control litter mates and normal mammary glands from transgenic mice were used as control normal tissue.

B7-H3-targeted Contrast-enhanced Ultrasound Imaging of Mice

Imaging Protocol—Mammary glands of transgenic mice bearing tumors (n=146) and normal control glands (n=37) were imaged. A detailed description of ultrasound molecular

imaging protocol is provided in the Supplementary Materials. Images representing signal from adherent MB (molecular imaging signal) were displayed as color maps on contrast-mode images, automatically generated by using commercially available Vevo CQ software (VisualSonics, Toronto, Canada). The scale for the color maps was kept constant for all images.

Assessment of Binding Specificity of B7-H3-Targeted Microbubbles In Vivo— To confirm binding specificity of $MB_{B7\text{-}H3}$ to B7-H3 expressed on the tumor neovasculature in transgenic mice, an intra-animal comparison of ultrasound imaging signal following intravenous injection of both 5×10^7 $MB_{B7\text{-}H3}$ and 5×10^7 $MB_{Control}$ in the same session was performed. For this purpose, mammary glands with breast cancer (n=10) were imaged using both $MB_{B7\text{-}H3}$ and $MB_{Control}$ in random order to minimize any bias from the injection order, and injections were separated by at least 30 minutes waiting time to allow clearance of microbubbles from previous injections (27). To further confirm binding specificity of $MB_{B7\text{-}H3}$ to B7-H3 in the same mice, targeted ultrasound imaging using $MB_{B7\text{-}H3}$ was repeated 5 hours after intravenous injection of 125 μg purified rat anti-mouse B7-H3 antibody (eBiosciences, San Diego, CA) to block B7-H3 receptor sites *in vivo*.

Data Analysis of In Vivo Imaging Data Sets—Imaging data sets of all mice were analyzed offline in random order using a dedicated workstation with commercially available software (Vevo 2100, Visualsonics, Toronto, Ontario, Canada). Analysis was performed in a blinded fashion by one of the authors. Since the transgenic mice used in this study can develop cancer as early as 4 weeks of age and morphological changes for these early invasive cancers are not visible on conventional B-mode ultrasound imaging (Figure 6) (28), this author was blinded to the mammary gland pathology (normal or cancer). The reader was also blinded to the microbubble type ($MB_{B7\text{-}H3}$ or $MB_{Control}$). Regions of interest (ROI) were drawn over the mammary glands and the magnitude of imaging signal (expressed in arbitrary units, a.u.) from attached microbubbles was assessed by calculating an average for pre- and post-destruction imaging signals and subtracting the average post-destruction signal from the average pre-destruction signal as described previously (19, 27, 29).

Ex Vivo Analysis of Mammary Glands from Transgenic Mice

Ex vivo histopathological and quantitative immunofluorescence analysis was performed using standard techniques (See Supplementary Materials).

Statistical Analysis

All data were expressed as mean ± standard deviation. For details on the statistical analysis please refer to Supplementary Methods

RESULTS

Validation of B7-H3 Expression in Human Breast Tissues

To assess B7-H3 expression in breast cancer-associated neovasculature in humans, immunohistochemical analysis was performed on breast tissues from a total of 248 women with normal breast tissue (n=47), 11 different benign and precursor breast pathologies

(n=100), and four different subtypes of breast cancer (n=101; Table 1). B7-H3 expression was detected on the cell membrane and within the cytoplasm of tumor epithelial cells, on fibroblast like cells within the stroma, as well as on membranes of vascular endothelial cells. Due to the vascular restriction of the ultrasound molecular contrast agent, only vascular staining (guided by vascular marker CD31 staining) was quantified. In 209 samples processed into a breast tissue microarray (TMA), B7-H3 expression was significantly ($P<0.001$) higher in breast cancer (mean composite score, 7.7) compared to normal tissue, benign and precursor breast lesions (mean composite score, 1.3; Figure. 2). Individual composite scores for all benign and malignant subtypes are shown in Figure. 3. A detailed summary of B7-H3 staining intensities and percent positive vessels in all normal, benign, premalignant and malignant human breast tissues is provided in Supplementary Table 1. Microvessel density was also significantly ($P<0.001$) increased in breast cancer versus normal, benign and precursor breast lesions (Figure. 4).

Considering a composite score of 4 or higher as positive staining, overall, 88/101 breast cancer, 17/100 benign lesions, and 6/47 normal tissues stained positive. Receiver operating characteristic (ROC) analysis indicated that B7-H3 neovascular immunostaining could distinguish breast cancer from normal tissue, benign and precursor lesions with an area under the ROC curve (AUC) of 0.90 (95% CI, 0.86, 0.94).

Since TMA represent only very small tissue samples of the various histologies, a sub-analysis of an additional 39 whole tissue samples of breast cancer was performed containing more representative amounts of respective tumor tissues and using the non-cancerous surrounding tissue as intra-individual benign controls. In these samples, the mean composite IHC score of malignant lesions (mean composite IHC score, 9.79) was significantly ($P<0.001$) higher compared to normal tissue, benign and precursor breast lesions (mean composite IHC score, 1.67; Supplementary Figure. 1 and Supplementary Table. 2). Considering a composite score of 4 or higher as positive staining, 39/39 breast cancer, 5/9 benign lesions, and 3/30 normal tissues stained positive. This corresponds to an AUC of 0.96 (95% CI, 0.92, 0.99) in differentiating cancer versus normal, benign and precursor lesions. Similarly, the microvessel density was significantly ($P<0.001$) increased in breast cancer versus normal tissue, benign and precursor lesions (Supplementary Figure. 2).

Flow Chamber Experiments

Microbubbles targeted to B7-H3 ($MB_{B7\text{-}H3}$) and control non-targeted microbubbles ($MB_{Control}$) were synthesized and binding specificity to B7-H3 was first tested in cell culture experiments. Figure. 5 illustrates binding of both $MB_{B7\text{-}H3}$ and $MB_{Control}$ to B7-H3 positive and negative mouse endothelial cells under flow shear stress conditions in a flow chamber. Average number of $MB_{B7\text{-}H3}$ attached per cell was significantly higher ($P<0.001$) on B7-H3 positive compared to negative cells. Blocking of the B7-H3 receptors with anti-B7-H3 antibodies resulted in significantly reduced ($P<0.001$) binding of $MB_{B7\text{-}H3}$ to B7-H3 positive cells, confirming binding specificity of $MB_{B7\text{-}H3}$ to B7-H3. There was only minimal non-specific binding of $MB_{Control}$ to B7-H3 positive cells compared to $MB_{B7\text{-}H3}$ ($P<0.001$).

B7-H3-targeted Contrast-enhanced Ultrasound Imaging in Transgenic Mice

Binding specificity of $MB_{B7\text{-}H3}$ to murine B7-H3 was first tested in 10 breast tumors in transgenic mice. *In vivo* ultrasound imaging signal obtained from $MB_{B7\text{-}H3}$ (36.6 ± 7.9 a.u.) was significantly higher ($P<0.001$) compared to the signal from $MB_{Control}$ (8.4 ± 3.6 a.u.). Furthermore, *in vivo* B7-H3-targeted ultrasound molecular imaging signal was significantly reduced (4.2 ± 1.6 a.u.; $P<0.001$) following administration of blocking anti-B7-H3 antibodies, further confirming *in vivo* binding specificity of $MB_{B7\text{-}H3}$ to the imaging target B7-H3 (supplementary Figure 3). We then studied whether ultrasound using B7-H3-targeted contrast microbubbles allows imaging of B7-H3 expression *in vivo* in 146 mammary glands bearing breast cancer and 37 normal mammary glands. Imaging signal in breast cancer following injection of $MB_{B7\text{-}H3}$ (49.4 ± 5.3 a.u.) was significantly higher ($P<0.001$) in breast cancer than in normal breast tissue (5.0 ± 0.5 a.u.) (Figure 6).

Ex Vivo Analysis

Similar to the human staining, B7-H3 expression was observed both on the tumor neovasculature and on tumor epithelial cells in mice (Figure. 6B). B7-H3 expression on breast cancer associated neovasculature was significantly ($P<0.001$) higher (mean intensity, 53 ± 28 a.u.) compared to normal breast tissue (mean intensity, 1.7 ± 1.1 a.u.). *Ex- vivo* B7-H3 expression levels as assessed on quantitative immunofluorescence correlated well ($R^2=0.77$, $P<0.001$) with *in vivo* B7-H3-targeted ultrasound imaging signal. Microvessel density was also significantly ($P<0.001$) higher in breast cancer (mean, 28 ± 16 vessels/mm^2) compared to normal mammary tissue (mean, 3 ± 4 vessels/mm^2).

DISCUSSION

Our immunohistochemical analysis of normal and a broad spectrum of different benign, premalignant and malignant breast pathologies in women undergoing surgical resection or biopsy shows that vascular endothelial cell expression of B7-H3 allows differentiation of breast cancer from benign entities with high diagnostic accuracy. Ultrasound molecular imaging signal in transgenic mice using B7-H3-targeted contrast microbubbles is substantially higher in breast cancer versus normal breast tissue.

In patients with dense breast tissues, ultrasound is currently being explored as a complementary imaging modality to screening mammography for breast cancer detection (7). Ultrasound is advantageous because it is widely available, cost-effective, does not expose patients to ionizing radiation, and allows real-time guided biopsy of sonographically detected lesions, if needed. General limitations of ultrasound as a screening tool, such as long imaging times and operator dependency, are already being addressed by the introduction of commercially available automated whole-breast ultrasound imaging systems that allow a time- and cost-efficient as well as more standardized acquisition and interpretation of breast ultrasound exams (30). In recent years, molecularly targeted ultrasound contrast agents have been developed to improve diagnostic accuracy of ultrasound in earlier detection of cancer such as pancreatic (15, 31), ovarian (32), and breast cancer (16, 19). To allow differentiation of cancer from non-cancerous tissue using ultrasound and molecularly-targeted contrast microbubbles, imaging targets have to be

differentially expressed on the neovasculature of cancer compared to vessels in non-cancerous tissue. Therefore, the goals of our study were, first, to explore whether a new potential molecular imaging target, B7-H3, is differentially expressed on the neovasculature of human breast cancer and, second, to assess binding specificity of a new B7-H3-targeted ultrasound contrast microbubble both in cell culture and *in vivo*.

B7-H3, a member of the B7 family of immunoregulators, was first identified on human dendritic cells and activated T cells (33, 34). Recently, B7-H3 expression has been shown in several cancer types including acute leukemia, gastric, pancreatic, renal, liver, lung, bone, colon, prostate, ovarian, endometrial, and breast cancer (35–47). However, its role in immune response, including tumor immunity of different cancer types, remains unclear and controversial (33, 48, 49). Both T-cell co-stimulatory and inhibitory functions have been shown in various cancer types and B7-H3 expression has been correlated with both favorable and poor prognosis in cancer patients (33, 35, 50). For example, in human gastric adenocarcinomas, B7-H3 expression was associated with prolonged patient survival compared to receptor negative tumors (50). In contrast, recent studies showed that B7-H3 tumor expression may be a predictor of poor prognosis and increased risk for metastasis in other cancers such as renal, colon, breast, and ovarian cancers (37, 41, 43, 46). In women with breast cancer, tumor expression of B7-H3 was suggested as a predictor of early regional lymph node metastases (47, 51), advanced stage disease (51), and overall worsened prognosis (43). Whether B7-H3 is expressed on the neovasculature of breast cancer and whether it can be used as new molecular imaging target for breast cancer with ultrasound remains unclear.

In 248 patient samples including normal, 11 different benign and precursor breast pathologies, and four subtypes of breast cancer, processed both in a tissue microarray and as whole tissue samples, we demonstrated that B7-H3 is overexpressed on breast cancer neovasculature compared to normal, benign and precursor breast pathologies, using a composite IHC score of both staining intensity and percentage of positively staining vessels. Considering a composite score of 4 or more (out of a maximum of 12) as positive staining, B7-H3 allowed differentiation of breast cancer from normal, benign and precursor lesions with high diagnostic accuracy. Since tissue microarrays only represent a very small sample of tumor or benign tissues, an IHC sub-analysis of 39 whole tissue breast cancer samples was also performed. In this subgroup, all breast cancer types showed positive B7-H3 staining on the neovasculature. Peri-tumoral breast tissues served as intra-individual controls and confirmed substantially less staining in normal, benign or precursor breast lesions associated with breast cancer.

After validation of B7-H3 as a potential vascular molecular imaging target for human breast cancer detection, B7-H3-targeted microbubbles were designed and tested both in cell culture experiments and *in vivo*. Flow chamber experiments simulating shear stress flow in tumor vessels confirmed binding specificity of B7-H3-targeted microbubbles to their molecular target. This was further confirmed in breast cancer imaging experiments *in vivo*, which showed substantially higher ultrasound molecular imaging signal in breast cancer following intravenous injection of B7-H3-targeted microbubbles compared to control microbubbles in intra-animal comparison experiments in the same breast cancers. Quantitative

immunofluorescence of excised murine mammary tissues further confirmed vascular expression of B7-H3 with excellent quantitative correlation between *in vivo* imaging signal and *ex vivo* expression levels of B7-H3. These results suggest that B7-H3-targeted ultrasound molecular imaging should be further developed as a non-invasive, relatively inexpensive imaging approach for breast cancer detection in patients.

We acknowledge the following limitations of our study. For this proof of principle imaging study in mice we used biotin-streptavidin binding chemistry and commercially available antibodies to generate B7-H3-targeted microbubbles. These were not intended for clinical use and ongoing experiments explore the design of clinical grade contrast microbubbles targeted at B7-H3 using techniques described previously (27, 52). Also, due to the small dimensions of murine breast tissues in the z-plane we chose to scan mice in two dimensional planes only in our study. Automatic whole breast scanners are now available in the clinic (30) which will facilitate future translation of volumetric ultrasound molecular imaging for screening purposes in patients. Finally, while we assessed breast cancer associated B7-H3 vascular endothelial cell expression in human tissue samples in a broad spectrum of benign and malignant breast lesions by immunohistochemistry, B7-H3-targeted ultrasound molecular imaging was only tested in normal and invasive breast cancer *in vivo*. To the best of our knowledge, there are no mouse models available that harbor the spectrum of all the benign diseases tested in the human samples in our study, which would allow modelling the diagnostic accuracy of B7-H3-targeted ultrasound molecular imaging in preclinical studies before translating this approach into the clinic. Therefore, future clinical studies using clinical grade B7-H3-targeted contrast microbubbles are warranted to both confirm our human IHC staining results and to assess diagnostic accuracy of ultrasound molecular imaging in detecting and characterizing breast cancer in patients.

In conclusion, our results suggest that B7-H3 is differentially expressed on the neovasculature of breast cancer compared to normal breast tissue and multiple benign breast pathologies in women undergoing surgical resection or biopsy. Ultrasound molecular imaging signal using contrast microbubbles targeted at B7-H3 is substantially increased in breast cancer versus normal breast tissue in transgenic mice. Future work towards clinical translation will develop clinical grade contrast agents targeted at B7-H3 that will eventually help in improving the diagnostic accuracy of ultrasound screening exams in detection and characterization of breast lesions in women with dense breast tissue

Supplementary Material

Refer to Web version on PubMed Central for supplementary material.

Acknowledgments

We would like to thank Ferdinand Knieling, visiting medical student from Erlangen in Germany, for his assistance with ultrasound imaging. We also acknowledge the support by Timothy Doyle, PhD in the Small Animal Imaging Facility at Stanford University.

Grant Support: This research was supported by the NIH R01 CA155289-01A1 grant (JKW) and by a Developmental Cancer Research Award from the Stanford Cancer Center (JKW).

Abbreviations

ADH	Atypical ductal hyperplasia
ALH	Atypical lobular hyperplasia
ApoM	Apocrine metaplasia
CCL	Columnar cell lesion
DCIS	Ductal carcinoma *in situ*
FA	Fibroadenoma
FEA	Flat epithelial atypia
NPFCC	Non-proliferative fibrocystic changes
UDH	Usual ductal hyperplasia
Her2	Human epidermal growth factor receptor type 2 positive cancer
Luminal A	estrogen receptor and/or progesterone receptor positive cancer
Luminal B	estrogen receptor and/or progesterone receptor positive and Her2 positive cancer
Triple negative	estrogen, progesterone and Her2 negative cancer
$MB_{B7\text{-}H3}$	B7-H3-targeted microbubbles
$MB_{Control}$	non-targeted microbubbles
MVD	microvessel density
ROC	receiver operating characteristic

References

1. Siegel R, Ma J, Zou Z, Jemal A. Cancer statistics, 2014. CA Cancer J Clin. 2014; 64:9–29. [PubMed: 24399786]
2. Smith RA, Manassaram-Baptiste D, Brooks D, Cokkinides V, Doroshenk M, Saslow D, et al. Cancer screening in the United States, 2014: a review of current American Cancer Society guidelines and current issues in cancer screening. CA Cancer J Clin. 2014; 64:30–51. [PubMed: 24408568]
3. Wang AT, Vachon CM, Brandt KR, Ghosh K. Breast Density and Breast Cancer Risk: A Practical Review. Mayo Clin Proc. 2014; 89:548–57. [PubMed: 24684876]
4. Berg WA, Zhang Z, Lehrer D, Jong RA, Pisano ED, Barr RG, et al. Detection of breast cancer with addition of annual screening ultrasound or a single screening MRI to mammography in women with elevated breast cancer risk. JAMA. 2012; 307:1394–404. [PubMed: 22474203]
5. Boyd NF, Guo H, Martin LJ, Sun L, Stone J, Fishell E, et al. Mammographic density and the risk and detection of breast cancer. N Engl J Med. 2007; 356:227–36. [PubMed: 17229950]
6. Kolb TM, Lichy J, Newhouse JH. Comparison of the performance of screening mammography, physical examination, and breast US and evaluation of factors that influence them: an analysis of 27,825 patient evaluations. Radiology. 2002; 225:165–75. [PubMed: 12355001]
7. Scheel JR, Lee JM, Sprague BL, Lee CI, Lehman CD. Screening ultrasound as an adjunct to mammography in women with mammographically dense breasts. Am J Obstet Gynecol. 2014

8. Buchberger W, Niehoff A, Obrist P, DeKoekkoek-Doll P, Dunser M. Clinically and mammographically occult breast lesions: detection and classification with high-resolution sonography. Semin Ultrasound CT MR. 2000; 21:325–36. [PubMed: 11014255]
9. Leconte I, Feger C, Galant C, Berliere M, Berg BV, D'Hoore W, et al. Mammography and subsequent whole-breast sonography of nonpalpable breast cancers: the importance of radiologic breast density. AJR Am J Roentgenol. 2003; 180:1675–9. [PubMed: 12760942]
10. Kaplan SS. Clinical utility of bilateral whole-breast US in the evaluation of women with dense breast tissue. Radiology. 2001; 221:641–9. [PubMed: 11719658]
11. Berg WA, Blume JD, Cormack JB, Mendelson EB, Lehrer D, Bohm-Velez M, et al. Combined screening with ultrasound and mammography vs mammography alone in women at elevated risk of breast cancer. JAMA. 2008; 299:2151–63. [PubMed: 18477782]
12. Hooley RJ, Greenberg KL, Stackhouse RM, Geisel JL, Butler RS, Philpotts LE. Screening US in patients with mammographically dense breasts: initial experience with Connecticut Public Act 09-41. Radiology. 2012; 265:59–69. [PubMed: 22723501]
13. Weinstein SP, Localio AR, Conant EF, Rosen M, Thomas KM, Schnall MD. Multimodality Screening of High-Risk Women: A Prospective Cohort Study. J Clin Oncol. 2009
14. Kiessling F, Fokong S, Koczera P, Lederle W, Lammers T. Ultrasound microbubbles for molecular diagnosis, therapy, and theranostics. J Nucl Med. 2012; 53:345–8. [PubMed: 22393225]
15. Foygel K, Wang H, Machtaler S, Lutz AM, Chen R, Pysz M, et al. Detection of pancreatic ductal adenocarcinoma in mice by ultrasound imaging of thymocyte differentiation antigen 1. Gastroenterology. 2013; 145:885–94. e3. [PubMed: 23791701]
16. Bachawal SV, Jensen KC, Lutz AM, Gambhir SS, Tranquart F, Tian L, et al. Earlier detection of breast cancer with ultrasound molecular imaging in a transgenic mouse model. Cancer Res. 2013; 73:1689–98. [PubMed: 23328585]
17. Wen Q, Wan S, Liu Z, Xu S, Wang H, Yang B. Ultrasound contrast agents and ultrasound molecular imaging. J Nanosci Nanotechnol. 2014; 14:190–209. [PubMed: 24730259]
18. Kiessling F, Fokong S, Bzyl J, Lederle W, Palmowski M, Lammers T. Recent advances in molecular, multimodal and theranostic ultrasound imaging. Adv Drug Deliv Rev. 2014; 72:15–27. [PubMed: 24316070]
19. Bzyl J, Lederle W, Rix A, Grouls C, Tardy I, Pochon S, et al. Molecular and functional ultrasound imaging in differently aggressive breast cancer xenografts using two novel ultrasound contrast agents (BR55 and BR38). Eur Radiol. 2011; 21:1988–95. [PubMed: 21562807]
20. Roesli C, Neri D. Methods for the identification of vascular markers in health and disease: from the bench to the clinic. J Proteomics. 2010; 73:2219–29. [PubMed: 20541635]
21. Seaman S, Stevens J, Yang MY, Logsdon D, Graff-Cherry C, St Croix B. Genes that distinguish physiological and pathological angiogenesis. Cancer Cell. 2007; 11:539–54. [PubMed: 17560335]
22. Turtoi A, Dumont B, Greffe Y, Blomme A, Mazzucchelli G, Delvenne P, et al. Novel comprehensive approach for accessible biomarker identification and absolute quantification from precious human tissues. J Proteome Res. 2011; 10:3160–82. [PubMed: 21534635]
23. Chandler I, Houlston R, Landberg G. A practical guide to constructing and using tissue microarrays. Methods Mol Biol. 2011; 675:363–73. [PubMed: 20949403]
24. Loos M, Hedderich DM, Ottenhausen M, Giese NA, Laschinger M, Esposito I, et al. Expression of the costimulatory molecule B7-H3 is associated with prolonged survival in human pancreatic cancer. BMC Cancer. 2009; 9:463. [PubMed: 20035626]
25. Weidner N. Current pathologic methods for measuring intratumoral microvessel density within breast carcinoma and other solid tumors. Breast Cancer Res Treat. 1995; 36:169–80. [PubMed: 8534865]
26. Guy CT, Cardiff RD, Muller WJ. Induction of mammary tumors by expression of polyomavirus middle T oncogene: a transgenic mouse model for metastatic disease. Mol Cell Biol. 1992; 12:954–61. [PubMed: 1312220]
27. Pochon S, Tardy I, Bussat P, Bettinger T, Brochot J, von Wronski M, et al. BR55: a lipopeptide-based VEGFR2-targeted ultrasound contrast agent for molecular imaging of angiogenesis. Invest Radiol. 2010; 45:89–95. [PubMed: 20027118]

28. Lin EY, Jones JG, Li P, Zhu L, Whitney KD, Muller WJ, et al. Progression to malignancy in the polyoma middle T oncoprotein mouse breast cancer model provides a reliable model for human diseases. Am J Pathol. 2003; 163:2113–26. [PubMed: 14578209]
29. Willmann JK, Paulmurugan R, Chen K, Gheysens O, Rodriguez-Porcel M, Lutz AM, et al. US imaging of tumor angiogenesis with microbubbles targeted to vascular endothelial growth factor receptor type 2 in mice. Radiology. 2008; 246:508–18. [PubMed: 18180339]
30. Giuliano V, Giuliano C. Improved breast cancer detection in asymptomatic women using 3D-automated breast ultrasound in mammographically dense breasts. Clin Imaging. 2013; 37:480–6. [PubMed: 23116728]
31. Pysz MA, Machtaler SB, Seeley ES, Lee JJ, Brentnall TA, Rosenberg J, et al. Vascular Endothelial Growth Factor Receptor Type 2-targeted Contrast-enhanced US of Pancreatic Cancer Neovasculature in a Genetically Engineered Mouse Model: Potential for Earlier Detection. Radiology. 2014:140568.
32. Lutz AM, Bachawal SV, Drescher CW, Pysz MA, Willmann JK, Gambhir SS. Ultrasound molecular imaging in a human CD276 expression-modulated murine ovarian cancer model. Clin Cancer Res. 2014; 20:1313–22. [PubMed: 24389327]
33. Wang L, Kang FB, Shan BE. B7-H3-mediated tumor immunology: Friend or foe? Int J Cancer. 2014; 134:2764–71. [PubMed: 24013874]
34. Vigdorovich V, Ramagopal UA, Lazar-Molnar E, Sylvestre E, Lee JS, Hofmeyer KA, et al. Structure and T cell inhibition properties of B7 family member, B7-H3. Structure. 2013; 21:707–17. [PubMed: 23583036]
35. Dai W, Shen G, Qiu J, Zhao X, Gao Q. Aberrant expression of B7-H3 in gastric adenocarcinoma promotes cancer cell metastasis. Oncol Rep. 2014
36. Zhao X, Li DC, Zhu XG, Gan WJ, Li Z, Xiong F, et al. B7-H3 overexpression in pancreatic cancer promotes tumor progression. Int J Mol Med. 2013; 31:283–91. [PubMed: 23242015]
37. Crispen PL, Sheinin Y, Roth TJ, Lohse CM, Kuntz SM, Frigola X, et al. Tumor cell and tumor vasculature expression of B7-H3 predict survival in clear cell renal cell carcinoma. Clin Cancer Res. 2008; 14:5150–7. [PubMed: 18694993]
38. Wang F, Wang G, Liu T, Yu G, Zhang G, Luan X. B7-H3 was highly expressed in human primary hepatocellular carcinoma and promoted tumor progression. Cancer Invest. 2014; 32:262–71. [PubMed: 24787022]
39. Wang L, Zhang Q, Chen W, Shan B, Ding Y, Zhang G, et al. B7-H3 is overexpressed in patients suffering osteosarcoma and associated with tumor aggressiveness and metastasis. PLoS One. 2013; 8:e70689. [PubMed: 23940627]
40. Roth TJ, Sheinin Y, Lohse CM, Kuntz SM, Frigola X, Inman BA, et al. B7-H3 ligand expression by prostate cancer: a novel marker of prognosis and potential target for therapy. Cancer Res. 2007; 67:7893–900. [PubMed: 17686830]
41. Zang X, Sullivan PS, Soslow RA, Waitz R, Reuter VE, Wilton A, et al. Tumor associated endothelial expression of B7-H3 predicts survival in ovarian carcinomas. Mod Pathol. 2010; 23:1104–12. [PubMed: 20495537]
42. Brunner A, Hinterholzer S, Riss P, Heinze G, Brustmann H. Immunoexpression of B7-H3 in endometrial cancer: relation to tumor T-cell infiltration and prognosis. Gynecol Oncol. 2012; 124:105–11. [PubMed: 21982044]
43. Maeda N, Yoshimura K, Yamamoto S, Kuramasu A, Inoue M, Suzuki N, et al. Expression of B7-H3, a Potential Factor of Tumor Immune Evasion in Combination with the Number of Regulatory T Cells, Affects Against Recurrence-Free Survival in Breast Cancer Patients. Ann Surg Oncol. 2014
44. Chen C, Shen Y, Qu QX, Chen XQ, Zhang XG, Huang JA. Induced expression of B7-H3 on the lung cancer cells and macrophages suppresses T-cell mediating anti-tumor immune response. Exp Cell Res. 2013; 319:96–102. [PubMed: 22999863]
45. Hu Y, Lv X, Wu Y, Xu J, Wang L, Chen W, et al. Expression of costimulatory molecule B7-H3 and its prognostic implications in human acute leukemia. Hematology. 2014

46. Bin Z, Guangbo Z, Yan G, Huan Z, Desheng L, Xueguang Z. Overexpression of B7-H3 in CD133+ colorectal cancer cells is associated with cancer progression and survival in human patients. J Surg Res. 2014; 188:396–403. [PubMed: 24630518]

47. Arigami T, Narita N, Mizuno R, Nguyen L, Ye X, Chung A, et al. B7-h3 ligand expression by primary breast cancer and associated with regional nodal metastasis. Ann Surg. 2010; 252:1044–51. [PubMed: 21107115]

48. Nygren MK, Tekle C, Ingebrigtsen VA, Fodstad O. B7-H3 and its relevance in cancer; immunological and non-immunological perspectives. Front Biosci (Elite Ed). 2011; 3:989–93. [PubMed: 21622107]

49. Loos M, Hedderich DM, Friess H, Kleeff J. B7-h3 and its role in antitumor immunity. Clin Dev Immunol. 2010; 2010:683875. [PubMed: 21127709]

50. Wu CP, Jiang JT, Tan M, Zhu YB, Ji M, Xu KF, et al. Relationship between co-stimulatory molecule B7-H3 expression and gastric carcinoma histology and prognosis. World J Gastroenterol. 2006; 12:457–9. [PubMed: 16489649]

51. Liu C, Liu J, Wang J, Liu Y, Zhang F, Lin W, et al. B7-H3 expression in ductal and lobular breast cancer and its association with IL-10. Mol Med Rep. 2013; 7:134–8. [PubMed: 23128494]

52. Pysz MA, Foygel K, Rosenberg J, Gambhir SS, Schneider M, Willmann JK. Antiangiogenic cancer therapy: monitoring with molecular US and a clinically translatable contrast agent (BR55). Radiology. 2010; 256:519–27. [PubMed: 20515975]

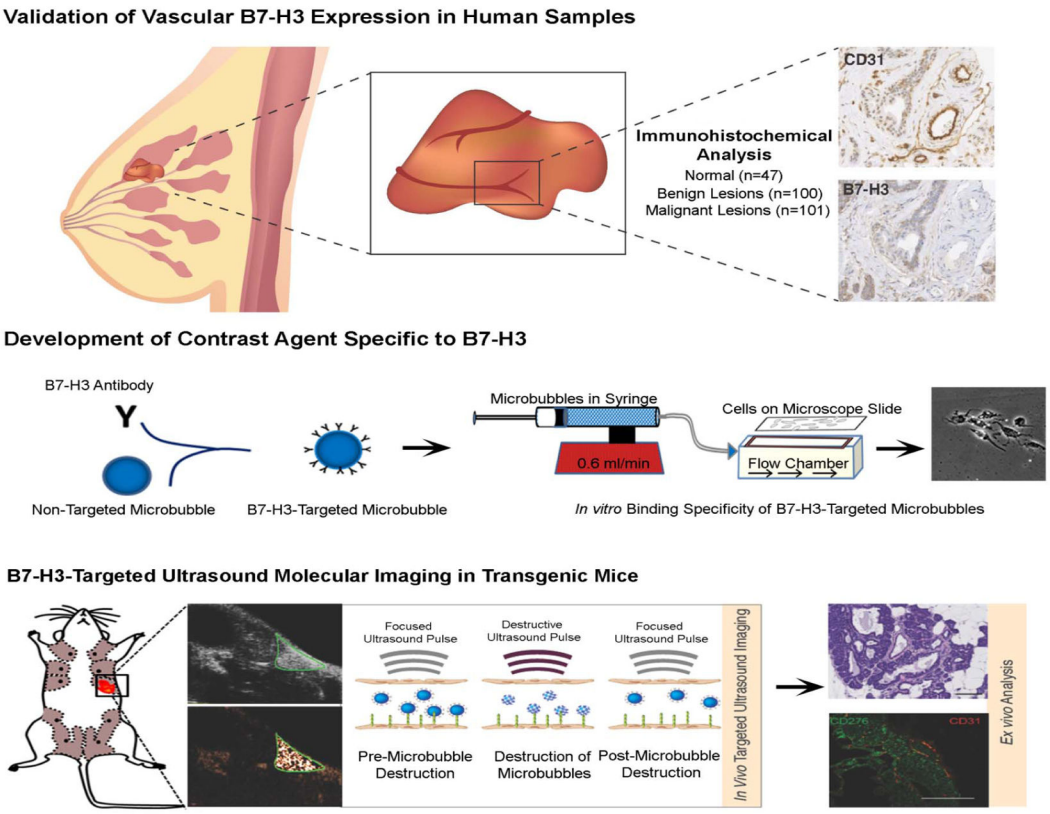

Figure 1. Summary of the overall study design

Differential expression of B7-H3 on breast cancer associated neovasculature was first assessed on a panel of normal, benign, premalignant and malignant breast lesions obtained from women undergoing biopsy or surgical resection. B7-H3-targeted contrast microbubbles were then generated, followed by testing both in cell culture and *in vivo* in a transgenic mouse model of breast cancer.

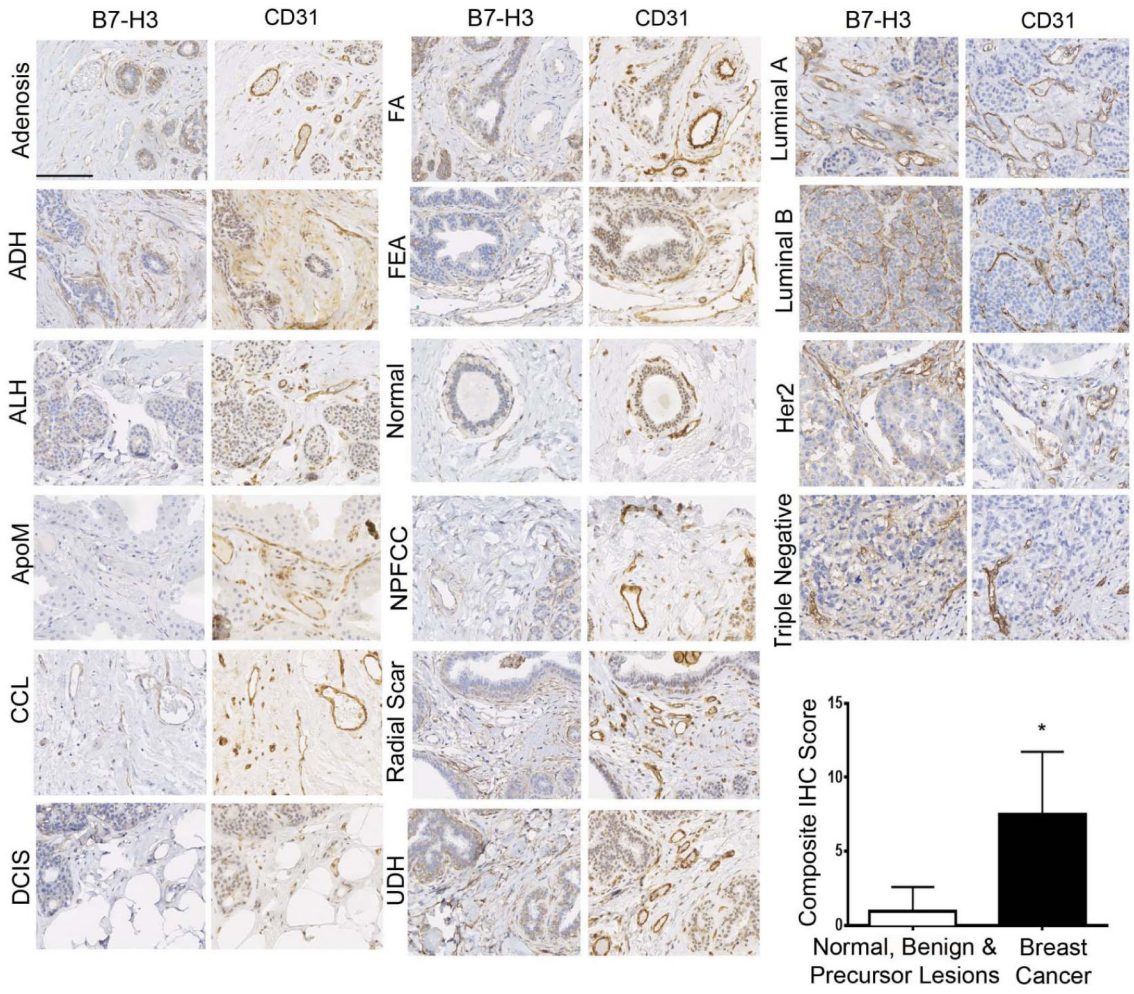

Figure 2. Immunohistochemical (IHC) analysis of B7-H3 expression in human breast tissues

Photomicrographs show representative staining results from normal breast tissues, various benign and precursor breast pathologies, as well as different types of breast cancer obtained from women undergoing biopsy or surgical resection. Graph summarizes composite IHC scores on B7-H3-stained tissues from normal tissue, benign and precursor lesions versus breast cancer. **P*<0.001; error bars = standard deviations, Scale bar = 100 μm. ADH=Atypical ductal hyperplasia; ALH=Atypical lobular hyperplasia; ApoM=Apocrine metaplasia; CCL=Columnar cell lesion; DCIS=Ductal carcinoma *in situ;* FA=Fibroadenoma; FEA=Flat epithelial atypia; NPFCC=Non-proliferative fibrocystic changes; UDH=Usual ductal hyperplasia; Her2=Human epidermal growth factor receptor type 2 positive cancer; Luminal A=estrogen receptor and/or progesterone receptor positive cancer; Luminal B=estrogen receptor and/or progesterone receptor positive and Her2 positive cancer; Triple negative=estrogen, progesterone and Her2 negative cancer.

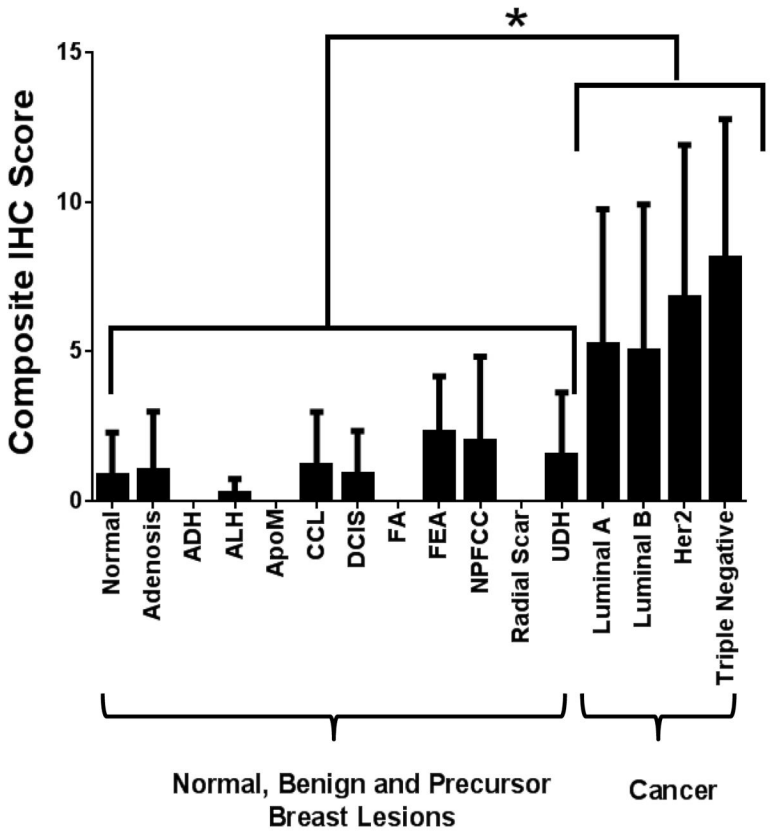

Figure 3. Composite IHC score

Summary of composite immunohistochemical (IHC) scores of B7-H3 staining of the vasculature in normal breast tissue, benign, premalignant, and malignant breast lesions. *P<0.001; error bars = standard deviations.

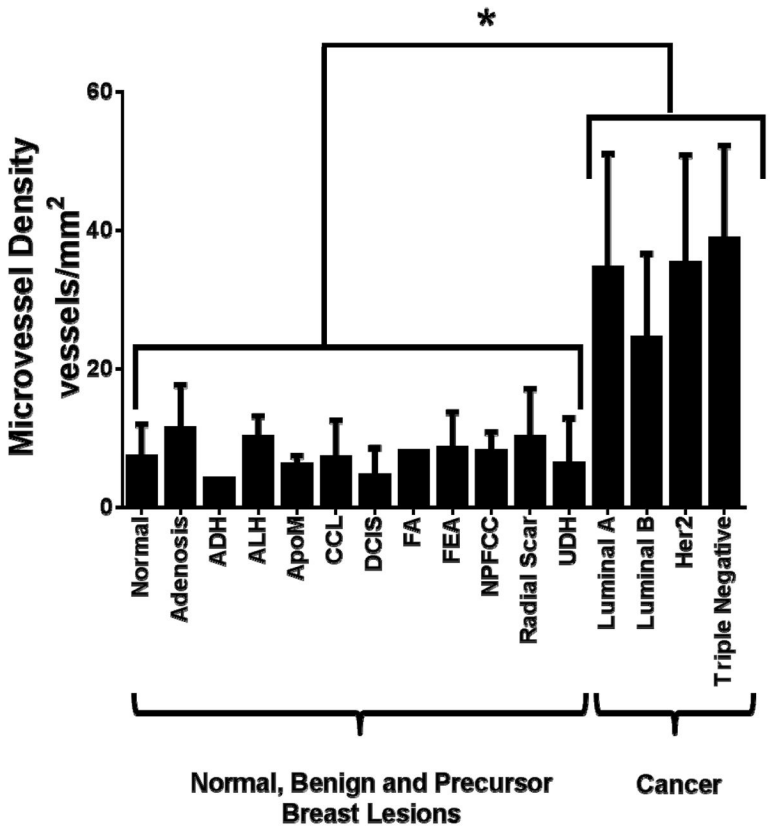

Figure 4. Microvessel density analysis

Summary of microvessel density (MVD) analysis on CD31 stained normal breast tissue, benign, premalignant and malignant lesions. *P<0.001; error bars = standard deviations.

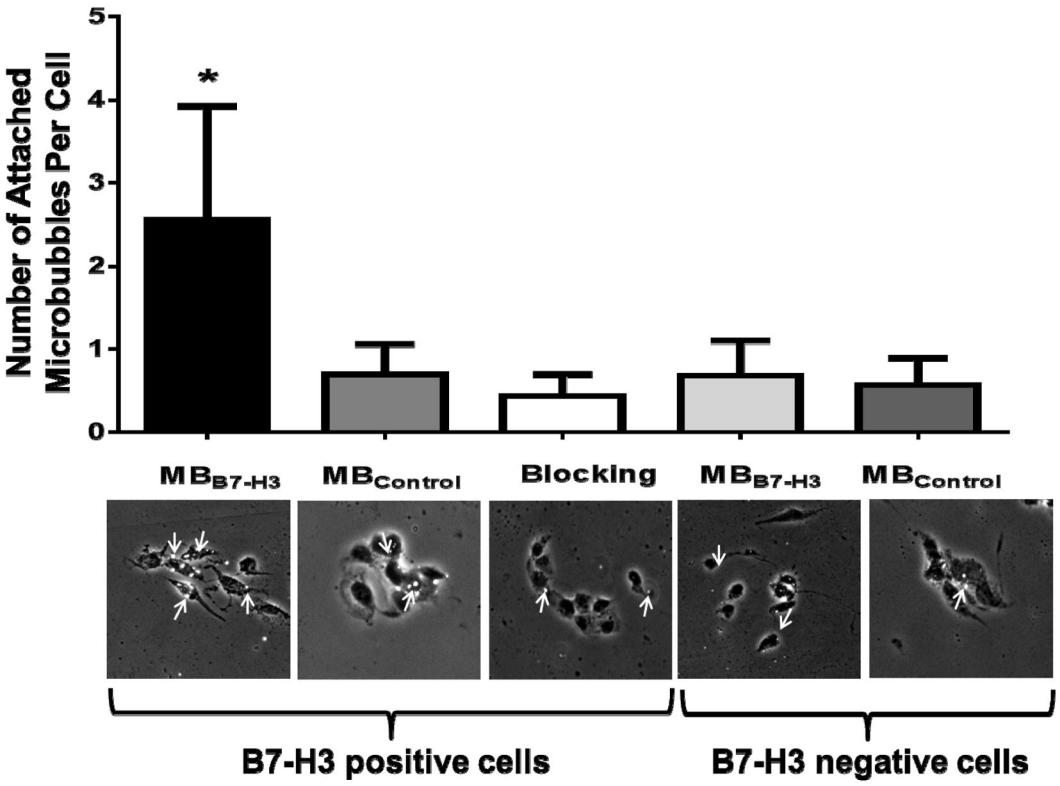

Figure 5. ***In vitro*** **binding specificity of B7-H3-targeted microbubbles**

Representative photomicrographs from cell culture experiments using a parallel plate flow chamber setting with B7-H3 positive and negative vascular endothelial cells, exposed to B7-H3-targeted microbubbles (of $MB_{B7\text{-}H3}$) and non-targeted control microbubbles (of $MB_{Control}$). Note specific attachment of $MB_{B7\text{-}H3}$ to B7-H3 positive cells and substantial binding inhibition following administration of blocking antibodies. Microbubbles (arrows) are visualized as white spherical dots.

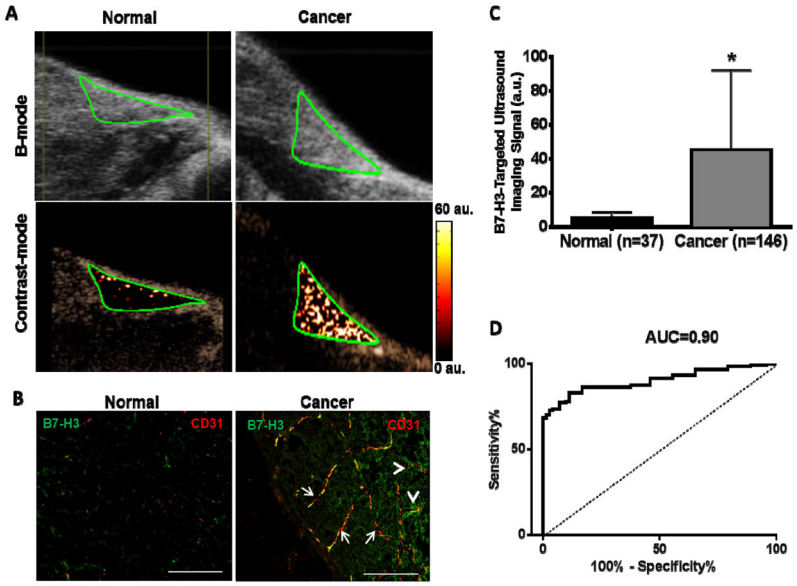

Figure 6. ***In vivo*** **ultrasound molecular imaging**

(A) Representative transverse B-mode and contrast mode ultrasound images following injection of B7-H3-targeted contrast microbubbles show strong signal in breast cancer and only background signal in a mammary gland with normal breast tissue (both outlined by a green region of interest). **(B)** Photomicrographs of immunofluorescence images (double stained for both the vascular marker CD31 (red) and B7-H3 (green)) confirm expression of B7-H3 on tumor neovasculature (arrows, yellow signal on merged images) in breast cancer with little to no vascular expression in normal tissue. Note B7-H3 is also expressed on tumor epithelium (arrowheads; green). **(C)** Bar graph summarizes quantitative B7-H3-targeted ultrasound molecular imaging signal obtained in normal and breast cancer in a total of 183 mammary glands with significantly increased imaging signal in breast cancer versus normal tissue. *P<0.001; error bars = standard deviations. **(D)** Receiving operator characteristic (ROC) curve in distinguishing normal from breast cancer based on quantitative ultrasound molecular imaging signal.

Table 1

Histological subtype and sample size

Summary of Various Breast Pathologies Collected and Analyzed by Immunohistochemistry.

Histology	Subtype	n
Normal Breast Tissue	N.A.	47
Benign and Precursor Breast Lesions	Adenosis	4
	ADH	1
	ALH	4
	ApoM	4
	CCL	57
	DCIS	10
	FA	1
	FEA	7
	NPFCC	2
	Radial scar	2
	UDH	8
Breast Cancer	Luminal A	45
	Luminal B	16
	Her2	19
	Triple negative	21

ADH=Atypical ductal hyperplasia; ALH=Atypical lobular hyperplasia; ApoM=Apocrine metaplasia; CCL=Columnar cell lesion; DCIS=Ductal carcinoma *in situ;* FA=Fibroadenoma; FEA=Flat epithelial atypia; NPFCC=Non-proliferative fibrocystic changes; UDH=Usual ductal hyperplasia; Her2=Human epidermal growth factor receptor type 2 positive cancer; Luminal A=estrogen receptor and/or progesterone receptor positive cancer; Luminal B=estrogen receptor and/or progesterone receptor positive and Her2 positive cancer; Triple negative=estrogen, progesterone and Her2 negative breast cancer.